

Electronic Supplementary Information

Stable Dispersions of Reduced Graphene Oxide in Ionic Liquids

Baoqing Zhang, Wei Ning, Jinming Zhang, Xin Qiao,

Jun Zhang, Jiasong He, Chen-Yang Liu

1. Samples preparation

1.1 Synthesis of Graphite Oxide

Graphite oxide was synthesized from expandable graphite (220–80 N of Grafguard Inc.) by a modified Hummers method.¹⁻³ In a typical experiment, expandable graphite powder (5 g) was put into cold (0 °C) concentrated H₂SO₄ (115 ml). Then, KMnO₄ (15 g) was added gradually with stirring and cooling, so that the mixture was kept to be below 20 °C. The mixture was then stirred at 35 °C for 4 hours. After this, distilled water (230 ml) was slowly added and caused an increase in temperature to 98 °C. The mixture was held at this temperature for 15 minutes without stirring. The reaction was terminated by addition of 700 ml distilled water. Shortly after the dilution, 30% H₂O₂ solution (30 ml) was added to the mixture, and the color of mixture changed into brilliant yellow along with bubbling. The mixture was filtered, washed successively with 5% HCl aqueous solution (500 ml) to remove metal ions followed by distilled water (500 ml) to remove acid. The resulting solid was vacuum dried at 60 °C and kept in desiccators for further use.

1.2 Preparation of suspensions of reduced graphene oxide (RGO) in ionic liquids (ILs)

Two kinds of ILs used in this study:

Two ILs with the cation of 1-alkyl-3-methylimidazolium:

- (i). 1-Butyl-3-methylimidazolium tetrafluoroborate (**BmimBF₄**)

(ii). 1-Allyl-3-methylimidazolium Chloride (**AmimCl**)

One IL with cation of N-alkylpyridinium:

(iii).N-Butylpyridinium tetrafluoroborate (**BpyBF₄**)

BmimBF₄ (i) and BpyBF₄ (iii) with the purity $\geq 99\%$ were obtained from Shanghai Chengjie Chemical Co. Ltd. and used as received. AmimCl (ii) was synthesized in our laboratory according to the procedure described in previous work.⁴

The typical procedure to prepare stable reduced graphene oxide (RGO)/ILs suspensions could be found in the main manuscript (schematically shown in **Fig.2**).

After chemical reduction, the obtained IL/RGO mixture with known weight was diluted in *N,N*-dimethylformamide (DMF), the solid filtered, and the filter cake washed with absolute alcohol for three times, vacuum heated at 80 °C for 2 days, then weighted to obtain the concentration of RGO. It was found that RGO concentration was about 70% of that of GO in unreduced IL/GO at present reduction condition.

The resulting BmimBF₄/RGO suspension (4.2 mg/ml, reduced from 6.0 mg/ml BmimBF₄/GO) was centrifuged at 10,000 rpm (~ 3,100g) for 2 hours, followed by carefully removing of supernatant liquid to isolate the gel phase. After the centrifugation, ~ 40.0 wt% of BmimBF₄ was removed. So the final concentration of RGO/BmimBF₄ gel was about 7.0 mg/ml. As the density of BmimBF₄ is ~1.20 g/ml at 25 °C, so the weight concentration of RGO for the gel is ~ 0.58%.

1.3 Preparation of Cellulose/RGO and PVDF/RGO nanocomposites

A dissolved pulp was used as cellulose origin to prepare the regenerated cellulose/RGO film sample. The viscosity-average degree of polymerization for dissolved pulp was about 650, which was measured by using an Ubbelodh viscometry method in cupriethylenediamine hydroxide solution. The fabrication procedure was very similar to a previous study.⁴ Cellulose sample with the weight of 2.62 g was added into 50 ml AmimCl/RGO suspension (0.53 mg/ml) in a flask, and the mixture

was heated at 80 °C and stirred for about 1 hour until cellulose was completely dissolved. The obtained solution was cast onto glass plates with the dimension of 15 × 15 cm², and took off air bubble in vacuum oven, and then coagulated in distilled water to obtain regenerated cellulose gel. The regenerated cellulose gel was immersed in distilled water bath to extract the remaining IL. The water was changed every 12 hours over the course of 3 days. The obtained cellulose/RGO (99/1 wt%) films were dried at 60 °C in vacuum oven before cutting and mechanical testing. The neat cellulose film samples were also prepared via similar procedure for comparison purpose.

In order to prepare PVDF/RGO nanocomposites, 4.2 mg/ml BmimBF₄/RGO suspension was firstly diluted by using DMF (200:1 corresponded to the volume of BmimBF₄). RGO was highly dispersible in DMF, and an ultrasound treatment for 20 minutes resulted in a light black solution stable for hours. PVDF (Kynar 740, Atofina Chemicals Inc.) with desired mass was then added to the above RGO solution. Ultrasound treatment and mild heating (40 - 50 °C) were combined to accelerate the dissolution of PVDF. The resulted DMF solutions were slowly added into a large volume of vigorously stirred methanol (5:1 with respect to the volume of DMF). The coagulated PVDF/RGO nanocomposite was filtered, washed with abundant methanol and dried at 80 °C under vacuum for about 24 h before further processing and characterization.

2. Instrumental characterizations

Wide-angle X-ray diffraction (WAXD) test was conducted by using a Rigaku D/max 2500 diffractometer with Cu K α ($\lambda = 0.15406$ nm) radiation (40 kV, 30 mA) with a 0.02 2 θ step and a 0.3 s count time.

Thermogravimetric analysis (TGA) was performed with a PE Pyris-1 thermogravimetric analyzer. The weight loss against temperature was measured from

30 °C to 750 °C in nitrogen atmosphere with a heating rate of 20 °C/min (for GO and RGO paper samples) or 10 °C/min (for PVDF/RGO composite).

X-ray photoelectron spectroscopy (XPS) data measurements of both GO and RGO paper samples were carried out with an ESCALab220i-XL electron spectrometer from VG Scientific using 300W Al K α radiation. The base pressure was about 3×10^{-9} mbar. The binding energies were referenced to the C_{1s} line at 284.8 eV.

The cross section of RGO paper sample was observed by using a JOEL JSM 6700F field-emission scanning electron microscope (SEM) operated at an accelerating voltage of 5 kV.

For IL/RGO suspensions (0.53 mg/ml), they were firstly diluted by using DMF (typically 200:1 respected to the volume of IL), and then were ultrasonically dispersed for 20 minutes before being deposited on freshly cleaved mica. Before atomic force microscopic (AFM) investigation, the deposited samples were allowed to dry in air at room temperature for two days. High-temperature drying was avoided because RGO always aggregated during heat-drying process. AFM images were taken in tapping mode with a Nano-Scope IIIA MultiMode apparatus (Digital Instruments). The height (topography) and phase images were recorded simultaneously.

GO aqueous dispersion (~ 0.01 mg/ml), as well as the diluted IL/DMF/RGO suspensions and were used for transmission electron microscope (TEM) imaging. The investigation was carried out by using a JEOL JSM-2200FS model TEM operated at 200 kV.

The regenerated cellulose and cellulose/RGO nanocomposite films with thickness of ~ 0.05 mm were cut into tensile samples with length and width of 50 and 7 mm, respectively. Tensile test was performed on an Instron universal testing machine with pneumatic clamps. The test conditions were room temperature and cross-head speed of 2 mm/min.

The rheological measurements were performed with a TA ARES-G2 strain-controlled rheometer under dry air conditions at 30 °C. The parallel plate geometry of 25mm or 50 mm radius was employed for the measurements.

3. Supporting Figures and Tables

3.1 Exfoliation of GO in water

As shown in **Fig. S1a**, the XRD pattern of natural graphite reveals a sharp peak at $2\theta = 26.4^\circ$, which corresponds to a *c*-axis spacing of 0.34 nm. The as-received expandable graphite (EG) displays two major 2θ peaks of 26.4° and 25.4° , which correspond to the original graphite crystal layer and the slightly expanded layer after acid-intercalation. Similar to the results of Cai and Song,³ our preliminary experiment showed that EG was easier to be oxidized compared to natural graphite. Thus an EG rather than natural graphite was used to prepare the graphite oxide in this study. The *c*-axis spacing of obtained graphite oxide increases to about 0.74 nm ($2\theta = 11.9^\circ$), and the 0.34 nm graphite interlayer spacing is completely eliminated by oxidation.

From the TEM photograph shown in **Fig. S1b**, it can be seen that graphite oxide was exfoliated into graphene oxide (GO) in aqueous media by ultrasonic treatment.

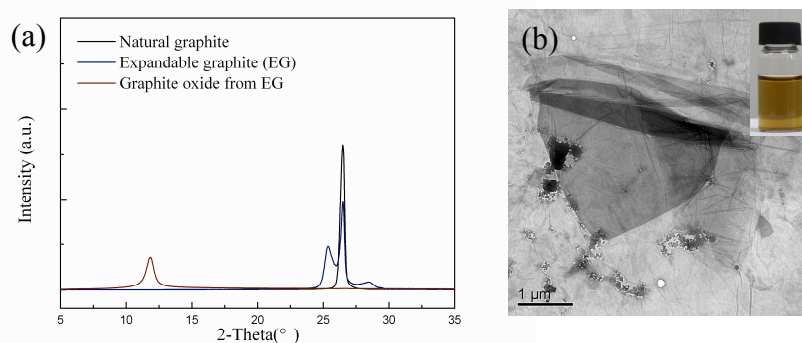


Fig. S1. Preparation of graphite oxide and its exfoliation in aqueous media. (a). WAXD patterns of natural graphite, as-received expandable graphite (EG) and prepared graphite oxide from EG; (b). TEM images of graphene oxide deposited onto a carbon coated copper mesh grid from an aqueous dispersion (inset).

3.2 How to understand the stabilization of both GO and RGO in selected ILs?

It is well accepted that graphene oxide sheet is hydrophilic and graphene sheet hydrophobic. Due to its strong polarity, water is the best molecular solvent to exfoliate graphite oxide and consequently form GO structure. There were also documents suggesting that graphite oxide could be fully exfoliated in some polar organic solvents, such as *N,N*-dimethylformamide (DMF), *N*-methyl-2-pyrrolidone (NMP),^{3,5} or the mixture of DMF/H₂O.⁶ It is safe to say that the strong polarity of solvent is one key factor for the exfoliation of graphite oxide and stable dispersion of GO in it. The polarities for selected ILs in this study are higher than that of DMF or NMP, as seen from Table S1, in which polarity is scaled by the empirical parameter of $E_T(30)$ or π^* . However, directly incorporating of graphite oxide in ILs, even based on lengthy sonication (> 24h), was failed to induce fully exfoliation and good dispersion of GO (**Fig. S2**).

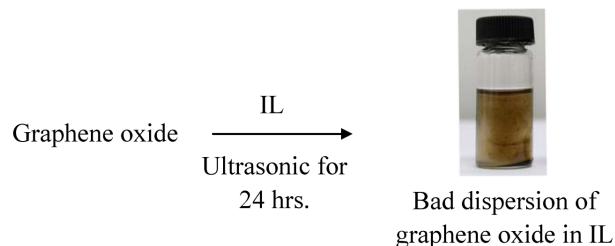


Fig. S2. Directly incorporating of graphite oxide in ILs was failed to induce good dispersion of GO.

Stimulated by the preparation method of Park et al.⁶ and the work that dealing with non-aqueous layered silicate suspensions,⁷ we also set off with GO aqueous suspension in the present study. After the exfoliation of graphite oxide in water with ultrasonic treatment, an IL was then added to the aqueous suspension. The agglomeration of GO occurred due to the suppression of electrostatic repulsion to stabilize GO particles. GO nanosheets could be re-dispersed in IL phase after removing H₂O under high vacuum with heating. All selected ILs possess relatively

high polarities and are miscible with H₂O. We believed that the good affinity between GO and selected ILs was responsible for the re-dispersion and stabilization of GO after removing H₂O.

Following the chemical reduction of GO in ILs, another question arising is that how to understand the stabilizing of hydrophobic reduced graphene oxide (RGO) in selected ILs? Recently, Coleman et al.⁸ tried to directly exfoliate natural graphite to stable graphene solution in a variety of organic solvents. They suggested that the matching of surface energies for graphite and solvent was one important criterion for successful exfoliation and further stabilization. Organic solvents were appropriate for this purpose when their surface tension in the range of 40 - 50 mJ/m².⁸ Generally speaking, surface tension values for ILs are higher than those of conventional organic solvents. For example, the surface tension of BmimBF₄ is 43.9 mJ/m² (25 °C).^{9a} This value meets the surface tension criterion and is somewhat higher than that of NMP (40.1 mJ/m²), while NMP has been testified as a good solvent for direct exfoliation for graphene.⁸ Park et al.⁶ also tried to correlated the stabilizing effect of RGO in a variety of organic solvents (organic solvent/H₂O mixtures actually) with two sets of solubility parameters (Hansen's and Kamlet–Taft's). Their preliminary conclusion was that RGO could be well dispersed in an organic solvent, when its sum of $\delta_p + \delta_h$ (δ_p , polarity cohesion parameter; δ_h , hydrogen bonding cohesion parameter) in the range of 13 ~ 29, or its $E_T(30)$ parameter in the range of 39 ~ 53. Because of lacking Hansen parameters for ILs, we just present the collected Kamlet–Taft solvent parameters in **Table S1** for three tested ILs. The corresponding parameters of water and two organic solvents (DMF and NMP) are also listed for comparison. It can be found that three ILs also satisfy the empirically $E_T(30)$ criterion that based on the testing of conventional organic solvents. All these suggest that our selected ILs have the possibility of working well in dispersing and stabilizing RGO just from

thermodynamics point, to say nothing of possible “cation- π ” and/or “ π - π ” interaction between graphite nanomaterials (carbon nanotube, graphene & nano-diamond) and ILs that has been confirmed by both experimental¹⁰ and simulation studies.¹¹

Table S1. $E_T(30)$ and Kamlet–Taft solvent parameters for selected ILs and molecular solvents at 25 °C

Solvents	$E_T(30)^a$ (kcal·mol ⁻¹)	Kamlet-Taft parameters ^b			Ref.
		α	β	π^*	
[Bmim]BF ₄	52.5	0.627	0.376	1.047	9c
[Amim]Cl	51.6 ^a	0.46	0.83	1.17	9d
[Bpy]BF ₄	51.4 (51.6 ^a)	0.523	0.213	1.081	9e,f
Water	63.1	1.17	0.18	1.09	--
DMF	43.2	0	0.69	0.88	--
NMP	43.8	0	0.77	0.92	--

a. The $E_T(30)$ value is considered to be a good general indication of the solvating ability of a liquid. It can be calculated from π^* and α based on following equation:

$$E_T(30)/\text{kcal}\cdot\text{mol}^{-1} = 31.2 + 11.5\pi^* + 15.2\alpha;^{9b}$$

b. π^* represents the solvent’s polarizability, and α and β are measures of the solvent’s hydrogen-bond donator acidity and hydrogen-bond acceptor basicity, respectively.^{9b}

3.3 SEM of resulted RGO paper

Similar to the aqueous RGO dispersion¹² and (DMF/H₂O)/RGO dispersion,⁶ our IL/RGO samples were also assembled to paper-like materials by using vacuum filtration method, and one obtained example is shown in **Fig. S3a**. As shown in **Fig. S3b**, SEM investigation of paper cross-sections showed a well-ordered layer structure for the RGO paper prepared from BmimBF₄/RGO suspension. This is also a complementary evidence for the well-dispersion of our IL/RGO samples, because bad dispersion is impossible to form the flexible paper-like sample presented here.

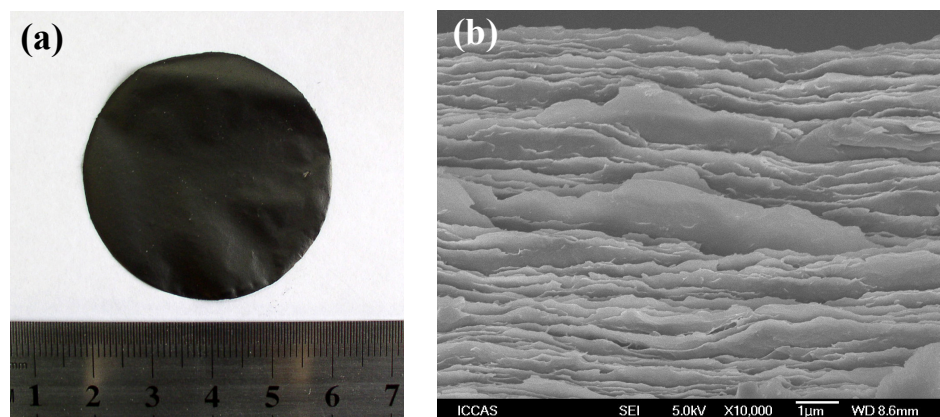


Fig. S3. (a). Digital photograph of RGO paper sample prepared by vacuum filtration method; (b) SEM photograph for its cross-section revealing the microscopic layered structure.

3.4 TGA and XPS results

The chemical changes occurring during the chemical reduction process were investigated by using TGA and XPS analyses. **Fig. S4a** shows the thermogravimetric (TG) and the derivative of thermogravimetric (DTG) curves for GO and RGO derived in BmimBF₄. The main mass loss observed for GO, which occurs around 200 °C can be ascribed to the pyrolysis of the labile oxygen-containing functional groups.^{13, 14} After reduction, this sharp mass loss around 200 °C is no longer observed. However, the mass loss over the whole temperature range above 200 °C is still preserved, which implies that the more stable oxygen functionalities are not eliminated. Similar results were observed for the RGO products obtained from hydrazine reduction process carried out in aqueous media.^{5, 12} The high resolution core level C1s XPS spectra of GO and RGO samples are presented in **Fig. S4b**. The elimination of oxygen functional groups for RGO sample can be easily identified by comparing the two

curves. The relative contribution assigned to oxygenated carbon species noticeably decreased as in the XPS spectra of RGO. The O/C atomic ratios derived from the XPS survey spectra (not shown here), which gave values of 0.40 for GO and 0.18 for the reduced one, also evidenced the successful de-oxygenation of the reduction process.

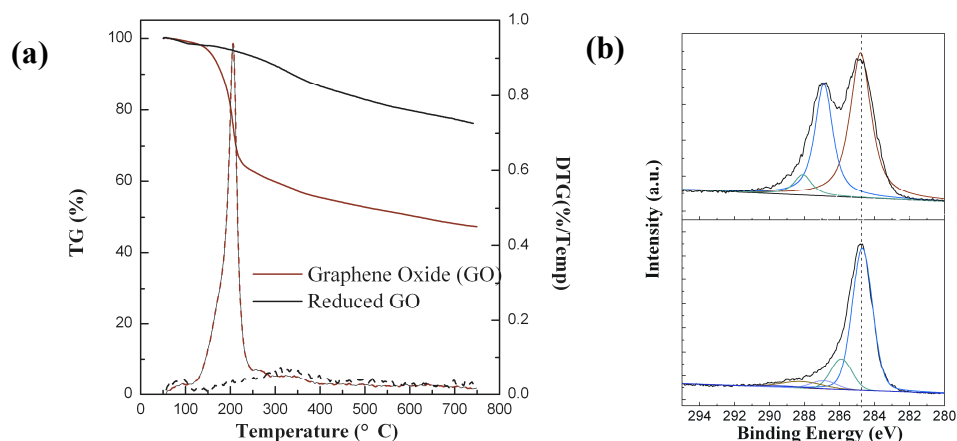


Fig. S4. (a) TG and DTG curves of GO and RGO derived in BmimBF₄; (b) High resolution C1s core level XPS spectra of GO (top), and RGO (bottom).

3.4 TEM images of RGO obtained by reduction in AmimCl and BpyBF₄

The black spots in TEM micrographs (**Fig. S5**) correspond to the residue IL particles, which due to its negligible vapor pressure, is impossible to evaporate in drying process after deposition of DMF/IL/RGO diluents on copper grid.

The multi-layer structure can be ascribed to the overlapping of already exfoliated graphene layers. We give this assessment based on the following reasoning: (i) the size of overlapped graphene sheet is of great difference, while in unexfoliated cases, the size difference of layers should be smaller; (ii) as shown in **Fig. S5b**, some IL particles are sandwiched between the graphene sheets, which further strengthening our idea that overlapping leads to the multi-layer structure in TEM samples.

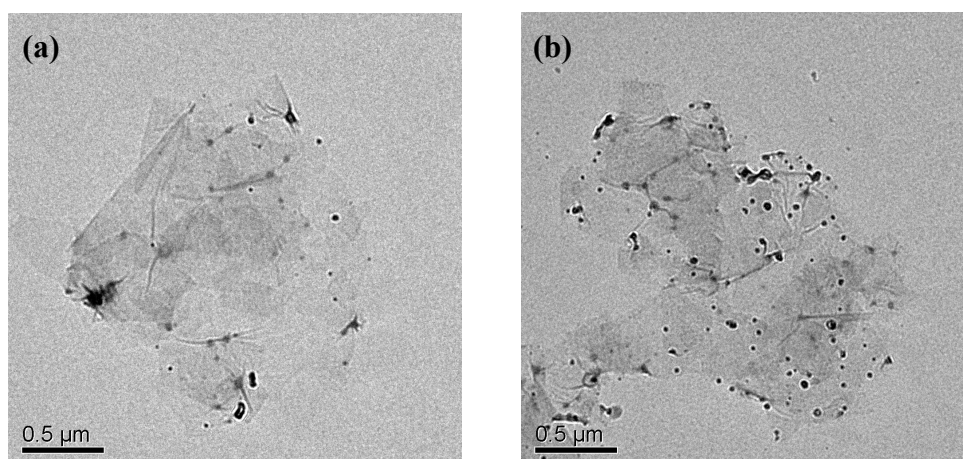


Fig. S5. TEM images for RGO obtained by diluting (a) AmimCl/RGO and (b) BpyBF₄/RGO in DMF.

3.6 Supplement results of rheological characterization

Fig. S6 shows the result of dynamic strain sweep test for BmimBF₄/RGO gel obtained by high-speed centrifugation. The gel shows a response of “weak strain overshoot”,¹⁵ i.e. above a critical yield strain, G' exhibits a power-law decrease, but G'' exhibits a peak before also falling in power-law manner. This strain-dependent nonlinear viscoelastic behavior is also a typical character of “soft glassy materials”.¹⁶ Furthermore, the yield stress was obtained from the curve of $\sigma \sim \gamma$, giving a value of ~ 50.0 Pa. This value is also comparable to the yield stress for the exfoliated clay/xylene suspension with a weight percent of 2.0% reported by Zhong & Wang.¹⁷ Considering the 2-D structure of graphene layer, together with the low solid concentration of our sample (~ 0.58 wt%), we think that the soft glassy rheological behavior is originated from the frictional interactions between RGO layers,¹⁸ most probably coupled with suspending IL medium, which accounts for the high effective particle volume fraction.

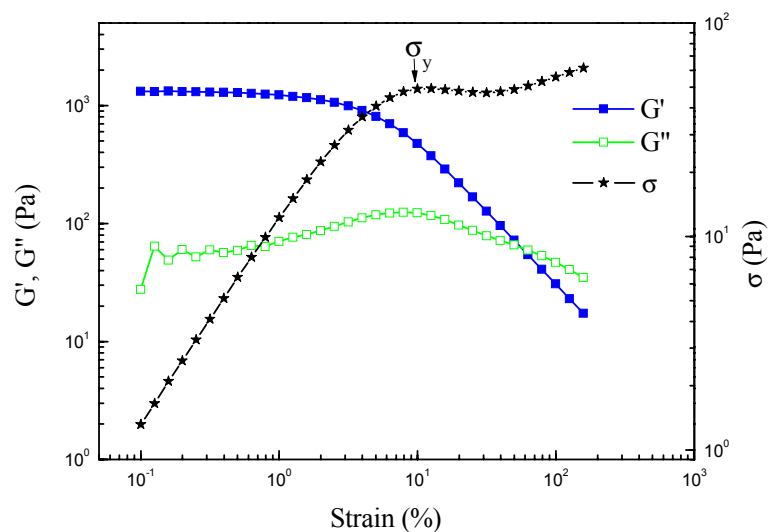


Fig.S6. Dynamic strain sweep at 1 rad/s of BmimBF₄/RGO gel obtained by high-speed centrifugation of 4.2 mg/ml BmimBF₄/RGO suspension.

The concentration-dependent dynamic viscoelastic behavior of AmimCl/RGO suspensions is shown in **Fig. S7**. Compared to the results of BmimBF₄/RGO (in the main text), it could be said that the rheological behaviors of IL/RGO suspensions also had certain relation with the type of ILs.

For both **Fig.4a** and **Fig. S7**, the data in the low frequency range for 0.21 mg/ml IL/RGO suspensions were removed because they were already not reliable as the measured torque in this range was too low and approached the low limit of torque rebalance of our rheometer.

$G' \sim \omega$ and $G'' \sim \omega$ curves for all three IL/RGO suspensions at the same weight concentration (2.1 mg/ml) are presented in **Fig. S8**. It is clear that RGO is more effective in increasing elasticity of dispersing IL phase for BmimBF₄ and BpyBF₄. Considering the very similar densities for three investigated ILs, the small differences of corresponding volume concentrations were not responsible for the divergences of rheological behaviors. At present, we still cannot give a credible explanation for such

a difference. A much more detailed investigation is deserved for understanding the rheological behaviors with relation to IL type, including a variety of cation and anion combinations, but it is beyond the scope of this study.

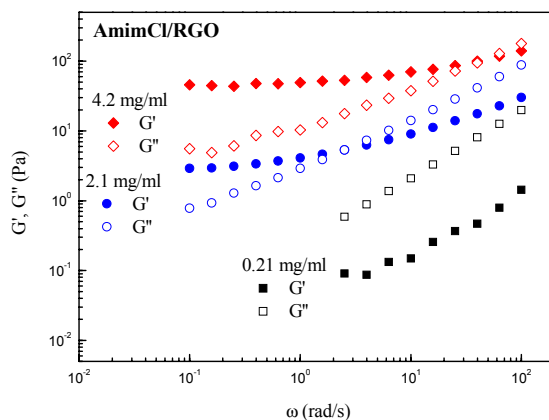


Fig. S7. Dynamic elastic (G') and viscous (G'') moduli as a function of oscillation frequency for AmimCl/RGO suspensions with different RGO concentrations.

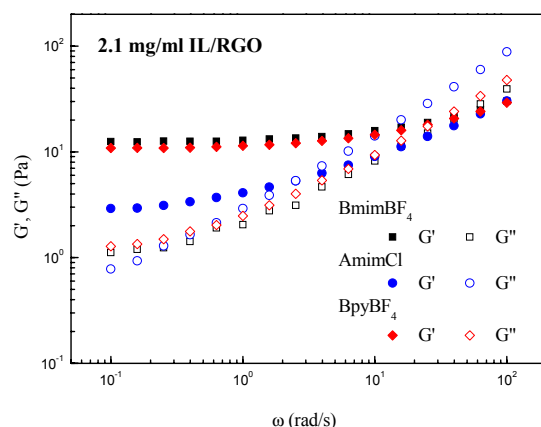


Fig. S8. Dynamic elastic (G') and viscous (G'') moduli as a function of oscillation frequency for 2.1 mg/ml RGO suspensions in three ILs.

After rheological characterization, the 2.1 mg/ml BpyBF₄/RGO sample was appropriately sealed and stored without any disturbance for about eight months. Then this stored suspension was used for the same oscillation frequency scanning test to check its stability over a long storage. The measurement result (denoted as **Stored**), combined with data extracted from **Fig. S8** (denoted as **As-prepared**), were plotted in **Fig. S9**. It can be seen that the reproducibility of rheological behaviors is quite good considering about eight months interval between the two tests, which confirms the

extra stability for BpyBF₄/RGO suspensions at least.

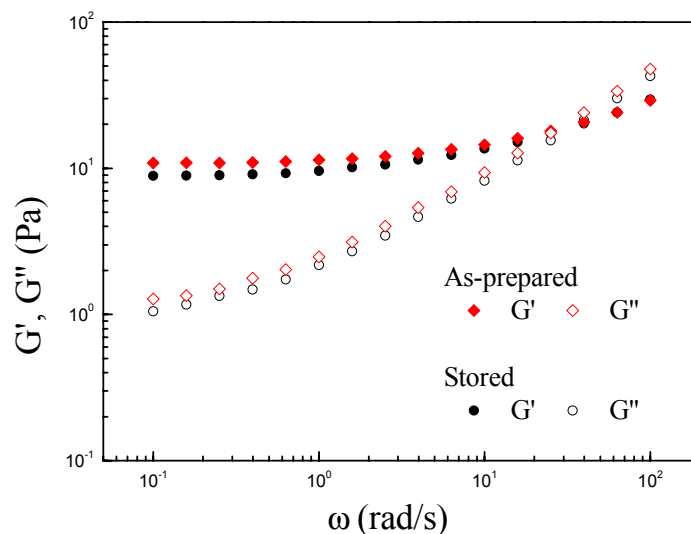


Fig. S9 Dynamic elastic (G') and viscous (G'') moduli as a function of oscillation frequency for 2.1 mg/ml BpyBF₄/RGO suspension before and after an eight-month storing.

3.6 Polymer/RGO nanocomposites

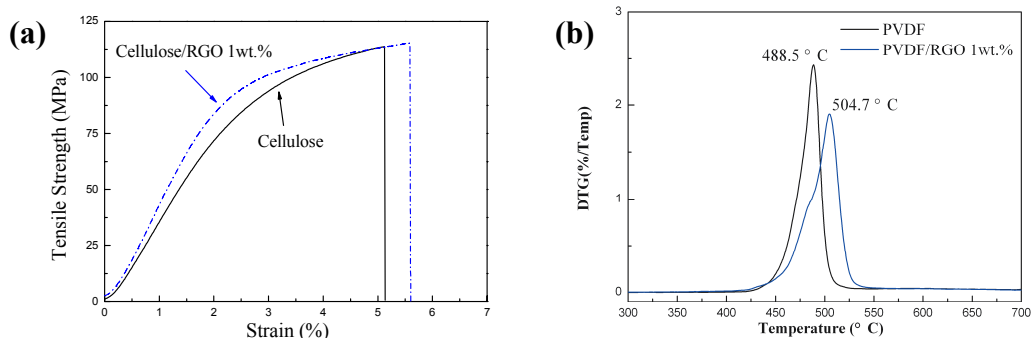


Fig. S10. (a) Typical stress–strain curves for cellulose (black) and cellulose-RGO nanocomposite (blue); (b) Derivative thermogravimetric (DTG) plots of pure PVDF (black) and PVDF/RGO nanocomposite (blue).

References for ESI

- (1) W. S. Hummers and R. E. Offeman, *J. Am. Chem. Soc.*, 1958, **80**, 1339.
- (2) P. G. Liu, K. C. Gong, P. Xiao and M. Xiao, *J. Mater. Chem.*, 2000, **10**, 933.
- (3) D. Y. Cai and M. Song, *J. Mater. Chem.*, 2007, **17**, 3678.
- (4) H. Zhang, J. Wu, J. Zhang and J. S. He, *Macromolecules*, 2005, **38**, 8272.

- (5) J. I. Paredes, SVillar-Rodil, AMartinez-Alonso and J. M. D. Tascon, *Langmuir*, 2008, **24**, 10560.
- (6) S. Park, J. H. An, I. W. Jung, R.D. Piner, S. J. An, X. S. Li, A. Velamakanni and R. S. Ruoff, *Nano. Lett.*, 2009, **9**, 1593.
- (7) C. Mobuchon, P.J. Carreau and M. C. Heuzey, *J. Rheo.*, 2009, **53**, 1025.
- (8) Y. Hernandez, V. Nicolosi, M. Lotya, F. M. Blighe, Z. Y. Sun, S. De, I. T. McGovern, B. Holland, M. Byrne, Y. K. Gun'ko, J. J. Boland, P. Niraj, G. Duesberg, S. Krishnamurthy, R. Goodhue, J. Hutchison, V. Scardaci, A. C. Ferrari and J. N. Coleman, *Nat. Nanotech.*, 2008, **3**, 563.
- (9) (a) Y. Wang, F. Y. Zhao, Y. M. Liu and Y. Q. Hu, *Acta. Chim. Sinica.*, 2007, **65**, 1443; (b) C. Reichardt, *Green Chem.*, 2005, **7**, 339; (c) L. Crowhurst, P. R. Mawdsley, J.M. Perez-Arlandis, P. A. Salter and T. Welton, *Phys. Chem. Chem. Phys.*, 2003, **5**, 2790; (d) Y. Fukaya, A. Sugimoto and H. Ohno, *Biomacromolecules*, 2006, **7**, 3295; (e) S. Park and R. J. Kazlauskas, *J. Org. Chem.*, 2001, **66**, 8395; (f) N.D. Khupse and A. Kumar, *J. Phys. Chem. B*, 2010, **114**, 376.
- (10) (a) T. Fukushima, A. Kosaka, Y. Ishimura, T. Yamamoto, T. Takigawa, N. Ishii and T. Aida, *Science*, 2003, **300**, 2072; (b) C. L. Park, A. Y. Jee, M. Y. Lee and S. G. Lee, *Chem. Comm.*, 2009, **37**, 5576.
- (11) (a) M. L. Sha, F. C. Zhang, G. Z. Wu, H. P. Fang, C. L. Wang, S. M. Chen, Y. Zhang and J. Hu, *J. Chem. Phys.*, 2008, **128**, 134504; (b) M. L. Sha, G. Z. Wu, H. P. Fang, G. L. Zhu and Y. S. Liu, *J. Phys. Chem. C*, 2008, **112**, 18584; (c) Y. S. Shim and H. J. Kim, *ACS Nano*, 2009, **3**, 1693.
- (12) D. Li, M. B. Muller, S. Gilje, R. B. Kaner and G. G. Wallace, *Nat. Nanotech.*, 2008, **3**, 101.
- (13) S. Stankovich, D. A. Dikin, R. D. Piner, K. A. Kohlhaas, A. Kleinhammes, Y. Jia, Y. Wu, S. T. Nguyen and R. S. Ruoff, *Carbon*, 2007, **45**, 1558.

- (14) J. I. Paredes, S. Villar-Rodil, P. Solis-Fernandez, A. Martinez-Alonso and J. M. D. Tascon, *Langmuir*, 2009, **25**, 5957.
- (15) K. Hyun, S. H. Kim, K. H. Ahn and S. J. Lee, *J. Non-Newton Fluid*, 2002, **107**, 51.
- (16) (a) T. G. Mason and D. A. Weitz, *Phys. Rev. Lett.*, 1995, **75**, 2770; (b) P. Sollich, F. Lequeux, P. Hebraud and M. E. Cates, *Phys. Rev. Lett.*, 1997, **78**, 2020; (c) H. M. Wyss, K. Miyazaki, J. Mattsson, Z. B. Hu, D. R. Reichman and D. A. Weitz, *Phys. Rev. Lett.*, 2007, **98**, 238303.
- (17) Y. Zhong and S. Q. Wang, *J. Rheo.*, 2003, **47**, 483.
- (18) G. Galgali, C. Ramesh and A. Lele, *Macromolecules*, 2001, **34**, 852.